sustainability

MDPI

Article

Active Collision-Avoidance Control Based on Emergency Decisions and Planning for Vehicle–Pedestrian Interaction Scenarios

Zexuan Han [1], Jiageng Ruan [1,*], Ying Li [1], He Wan [1], Zhenpeng Xue [1] and Jinming Zhang [2]

[1] College of Mechanical and Energy Engineering, Beijing University of Technology, Beijing 100020, China; hanzx@emails.bjut.edu.cn (Z.H.); lygogogo@emails.bjut.edu.cn (Y.L.); wanhe1105@emails.bjut.edu.cn (H.W.); xuezp@emails.bjut.edu.cn (Z.X.)

[2] School of Intelligent Manufacturing, Weifang University of Science and Technology, Weifang 262700, China; zhangjinming@wfust.edu.cn

* Correspondence: ruanjiageng@bjut.edu.cn; Tel.: +86-178-1318-8160

Abstract: Safe driving and effective collision avoidance are critical challenges in the development of autonomous driving technology. As the dynamic interactions between vehicles and pedestrians become increasingly complex, making rational decisions and accurately executing planning and control in emergency situations has become a core issue for sustainable development relating to traffic mobility and safety. This paper proposes an active collision-avoidance control strategy based on emergency decisions and planning in the context of vehicle–pedestrian interactions. A safety-distance model is developed with consideration given to the dynamic interactions between these two entities, and an emergency-decision mechanism is designed using the integration of priority rules. To generate smooth collision-avoidance trajectories, a quintic polynomial method is employed to construct trajectory clusters that meet the desired specifications. Moreover, a multi-objective optimization value function which considers multiple factors comprehensively is used to select the optimal path. To enhance collision-avoidance control accuracy, an RBF (radial basis function)–optimized SMC (sliding mode control) algorithm is introduced. Additionally, an FD-SF (force demand–based speed feedback) algorithm is designed to accurately track the longitudinal braking path. The results indicate that the proposed strategy can generate efficient, comfortable, and smooth optimal collision-avoidance paths, significantly improving vehicle response speed and control accuracy.

Keywords: intelligent vehicle; emergency decision; path planning; collision avoidance; interaction scenario; sustainable traffic

check for updates

Academic Editor: Lihui Zhang

Received: 4 January 2025
Revised: 18 February 2025
Accepted: 24 February 2025
Published: 26 February 2025

Citation: Han, Z.; Ruan, J.; Li, Y.; Wan, H.; Xue, Z.; Zhang, J. Active Collision-Avoidance Control Based on Emergency Decisions and Planning for Vehicle–Pedestrian Interaction Scenarios. *Sustainability* **2025**, *17*, 2016. https://doi.org/10.3390/su17052016

Copyright: © 2025 by the authors. Licensee MDPI, Basel, Switzerland. This article is an open access article distributed under the terms and conditions of the Creative Commons Attribution (CC BY) license (https://creativecommons.org/licenses/by/4.0/).

1. Introduction

With the rapid development of autonomous driving technology, ensuring driving mobility and safety has become one of the core challenges in this field. Autonomous driving systems must be capable of making swift and precise judgments in complex traffic environments to avoid potential collision risks. Among the various traffic participants, pedestrians, due to their unpredictable behavior characteristics, have become a key focus for autonomous driving systems. Especially on complex urban roads, or in high-density traffic scenarios, the dynamic interactions between vehicles and pedestrians are more frequent and fraught with uncertainty. How to make timely and effective decisions and how to plan the execution of collision-avoidance control operations in emergency situations have become crucial issues in the work to enhance the safety and comfort of autonomous

driving. The effective resolution of this issue holds significant importance for promoting the sustainable development of transportation systems.

As a key component in autonomous driving systems, mode decision plays a crucial role in ensuring that vehicles can accurately and smoothly complete various driving tasks [1–3]. Mode decision can be primarily categorized into two types: machine learning-based methods and rule-based methods. Machine learning-based decision-making methods analyze large amounts of driving data, extract key factors that influence driving behavior, and use these for model training to achieve decision-making. References [4,5] employed imitation and reinforcement learning methods to train upon and simulate human driver-control behaviors for decision-making. Reference [6] utilized the SVM (Support Vector Machine) algorithm and Bayesian optimization for training, constructing an autonomous lane-changing decision model that considers benefits, safety, and tolerance. References [7,8] proposed a lane-changing decision model that integrates multiple factors such as surrounding vehicle speeds, positioning information, and vehicle distances. References [9,10] combined the IAMPDM method with a collaborative decision-making framework to characterize the interactions between pedestrians and vehicles. And by incorporating an explicit prediction model and decision loop, the approach effectively addresses interaction issues under specific conditions. And neural network learning methods are used in complex decision-making scenarios. In recent years, scholars have adopted deep reinforcement algorithms such as DQN (Deep Q-Network) [11,12] and DDQN (Dueling Deep Q-Network) [13] to accomplish vehicle decision-making behaviors. Although machine learning has made some progress in the field of decision-making, existing technologies still face computational constraints. When integrated with planning and control, these constraints may result in response delays. Emergency collision-avoidance scenarios necessitate the full assurance of safety and real-time performance. Consequently, the implementation of these methods in complex and sudden real-world situations is difficult. In contrast, the necessity and feasibility of behavior are evaluated through road information and vehicle status by the rule-based decision-making method. These methods offer advantages such as simple principles, good real-time performance, and high reliability. As a result, this approach remains the mainstream choice at present. References [14,15] further explored research directions for lane-changing decision, utilizing derivatives of the Artificial Potential Field theory. Reference [16] employs conditional random fields to assess the risk levels associated with surrounding traffic participants in order to make decisions. Reference [17] uses ADS (Accumulated Driving Dissatisfaction) as the basis for lane-change decisions. Reference [18] establishes a pedestrian crossing direction probability model and a position-prediction model and implements decision-making by establishing a safety distance for turning for collision avoidance. However, existing methods have not fully taken into account factors such as the status and distance of obstacles, which may lead to reduced traffic efficiency and reliability after collision avoidance is performed. Furthermore, these methods often overlook the impacts of pedestrians. Due to the highly uncertain and complex nature of pedestrian behavior, relying solely on existing methods is insufficient when effectively navigating dynamic and complex traffic scenarios.

In recent years, the academic community has proposed various solutions to address the issues of path planning and collision-avoidance control in autonomous driving systems. In the field of local path planning under emergency conditions, Reference [19] introduced a novel DRRT (Dynamic Rapidly-Exploring Random Tree) method, incorporating kinematic constraints to prune redundant search points. To tackle the problems of slow convergence and non-optimal paths in traditional RRT methods, References [20,21] proposed improved approaches that combine random sampling, nearest neighbor search, and path optimization algorithms. However, these methods may lead to the exploration of extraneous areas,

subsequently reducing the algorithm's real-time performance and generating unstable paths. Graph-based search methods typically regularize and discretize feasible regions and utilize search algorithms to compute viable paths. Typical algorithms include the Hybrid A* planning method [22] and the Dijkstra [23] search algorithm. Nonetheless, these methods rely on complete graph-structure information, and struggle to quickly adapt and update paths in the face of dynamically changing obstacles. Reference [24] proposed a danger repulsive-force-field model for vehicle collision scenarios. Reference [25] introduced an improved Newton's method to address the inherent oscillation issues of potential field methods in the presence of obstacles and narrow passages. In response to the limitations of the traditional APF (Artificial Potential Field) method in complex scenarios, Reference [26] discarded the influence of the traditional force field and established the E-APF (Enhanced Artificial Potential Field) method by discretizing the shapes of obstacles. However, these methods rely on the accurate construction of the potential-obstacle field, which results in high computational costs and a tendency to fall into local minima. In the context of curve fitting methods, References [27,28] achieved personalized lane changing utilizing the sinusoidal lane-changing trajectory model and the hyperbolic tangent function model; additionally, acceleration limits were introduced to enhance passenger comfort. Reference [29] proposed a polynomial planning approach that considered the impact of the leading vehicle and optimized parameters through nonlinear programming. Nonetheless, these methods do not fully account for real-world conditions, vehicle dynamic constraints, and the impact of lane changes on surrounding traffic, leading to lower adaptability and safety in practical applications.

The research on collision avoidance and tracking control aims to maintain a safe distance between the vehicle and other traffic participants through precise control algorithms. Traditional tracking control methods are typically based on classical control theories, such as PID control, fuzzy control, sliding mode control, linear quadratic regulator control, model predictive control, etc. [30,31]. However, due to the highly dynamic nature of traffic environments, traditional methods often face issues such as delayed response and insufficient control accuracy when dealing with sudden situations. Therefore, in recent years, scholars have made various improvements and optimizations to these methods. Reference [32] optimized the weight matrix in traditional LQR control by using PSO (Particle Swarm Optimization), further enhancing control performance. Reference [33] introduced multi-point preview for road curvature within a finite time window into the augmented state vector, proposing an augmented LQR tracking algorithm utilizing optimal preview control. Reference [34] considered the effects of tire slip and actuator torque on vehicle acceleration/braking and designed a differential steering–dynamic sliding mode controller that resists integral saturation. The same reference [35] also proposed an adaptive model predictive path-tracking controller whose model parameters can be dynamically adjusted according to measurement data. References [36,37] provided a more precise modeling of the steering system and verified the effectiveness of the RMPC algorithm in emergency scenarios. However, the control accuracy of these methods relies on the vehicle model used, and model errors may lead to a decline in control effectiveness in actual scenarios. Particularly in complex and dynamic environments, inaccuracies in the model exacerbate control deviations, thereby reducing the effectiveness of the system in practical applications. In recent years, with the rapid development of artificial intelligence technologies, collision-avoidance control methods utilizing neural networks have gradually come into use. This method offers a more intelligent, precise, and efficient solution for collision-avoidance control in complex traffic environments through real-time training on driving data.

To address the issues present in the existing research, and promote the development of sustainable transportation systems in a safer, more efficient, and more environmentally friendly direction, this paper proposes an integrated strategy for active collision-avoidance control based on emergency decisions and planning for vehicle–pedestrian interaction scenarios. This strategy initially establishes a safety-distance model according to the dynamic interaction between vehicle and pedestrian. Subsequently, an emergency collision-avoidance decision mechanism for steering and braking is designed, incorporating priority rules for different operating conditions. In terms of path planning, a quintic polynomial method is employed to generate smooth collision-avoidance paths that comply with dynamic vehicle constraints. These paths are then evaluated and selected using a multi-objective optimized value function to determine the optimal collision-avoidance reference trajectory. Finally, to enhance the accuracy, stability, and robustness of the collision-avoidance control, an SMC algorithm optimized with RBF is introduced.

The comparative assessments and innovations of this study relative to the related research are shown in Table 1; the main contributions are as follows:

(1) A multi-mode emergency-decision mechanism based on a safety-distance model is proposed which can make real-time decisions for steering or braking in complex interaction scenarios.
(2) By combining the quintic polynomial method with a multi-objective optimization function, an efficient and comprehensive solution is provided for collision-avoidance path planning.
(3) The accuracy and stability of collision-avoidance control are enhanced through the RBF-SMC algorithm, further promoting the application of autonomous driving systems in pedestrian interaction environments.

Table 1. Comparisons and relative innovations for this study and the related research.

Previous Research	Current Research
Insufficient adaptability to the scene and limited computing power	Considers dynamic interactive scenarios to improve real-time performance
Less consideration of varying factors and the need to improve path stability	Takes into account multiple factors, and is more in line with actual needs
Focus on optimizing and improving traditional control methods	Introduces neural networks with improved adaptability and robustness
Focus on the making of single decisions, planning, and the control algorithm	Considers decisions in terms of the whole and considers them from multiple perspectives and angles

2. Mode Decision Based on a Safety-Distance Model

During normal vehicle driving, when a pedestrian appears ahead, appropriate steering or braking measures must be taken, taking into account the actual situation, to avoid the risk of collision. Existing methods typically focus on collision avoidance relative to vehicles and static obstacles, and rely on predefined rules and fixed thresholds for decision-making. When dealing with complex, real-time decision-making scenarios, their lack of flexibility can limit the efficiency and accuracy of the decisions.

In response to the time-varying and uncertain nature of vehicle–pedestrian interaction environments, this paper establishes a safety-distance model that considers instantaneous states, in order to dynamically adjust the scope of the application of rules. This model sets priorities according to specific parameters to support the implementation of an emergency-decision mode. Through this adaptive mechanism, the vehicle can promptly assess risks and take corresponding measures in dynamic environments, thereby ensuring driving safety.

2.1. Steering/Braking Safety-Distance Model

To calculate the safety distance in vehicle–pedestrian interactions, it is first necessary to analyze the road scenario according to actual conditions. Assume the vehicle is being driven in a straight line along the centerline of the road at longitudinal speed v_{hx}. At this moment, the pedestrian at point x_p ahead is crossing the road at speed of v_p. To simplify the problem, factors such as road surface irregularities, variations in road friction, and uncertainties in pedestrian behavior are neglected. Make the center of mass of the vehicle the origin of the coordinate system. Its driving direction and vertical road centerline direction are, respectively, the positive directions of the X-axis and Y-axis, establishing the road scene. The specific details are shown in Figure 1.

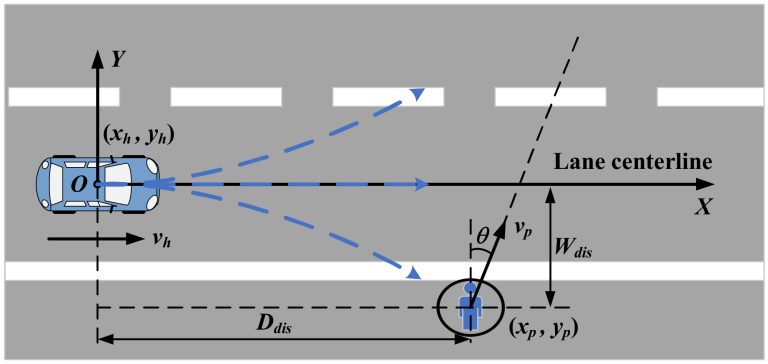

Figure 1. Information relative to a road scene interaction between vehicle and pedestrian.

In the aforementioned road scenario, the initial lateral velocity v_{hy} of the vehicle is zero, and the pedestrian is moving in an uncertain direction and at varying speeds. In the absence of braking, steering can rapidly adjust the vehicle's lateral trajectory. This not only enables effective collision avoidance but also maintains speed stability, demonstrating higher flexibility and adaptability. It is assumed that the vehicle's longitudinal speed remains constant during the steering process. Moreover, the lateral displacement of the vehicle should be minimized as much as possible when avoiding a collision. Considering the relative motion state relationship and the corresponding kinematic equation, the following formula must describe the interaction between the vehicle and the pedestrian:

$$\begin{cases} y_p + \left(v_p \frac{D_{dis}}{v_{hx}} + \frac{1}{2} a_p \left(\frac{D_{dis}}{v_{hx}}\right)^2\right) \cos\theta - W_{safe} = -\frac{1}{2} a_{hy} t_{steer}^2, W_{safe} > y_f \geq 0 \\ y_p + \left(v_p \frac{D_{dis}}{v_{hx}} + \frac{1}{2} a_p \left(\frac{D_{dis}}{v_{hx}}\right)^2\right) \cos\theta + W_{safe} = \frac{1}{2} a_{hy} t_{steer}^2, -W_{safe} < y_f < 0 \end{cases} \quad (1)$$

In the formula, y_p, v_p are the initial lateral position and initial travel speed of the pedestrian. D_{dis} is the longitudinal distance between the vehicle and the pedestrian at the initial moment. The a_p is the acceleration of the pedestrian during crossing. The θ is the angle between the pedestrian's crossing speed and the axis direction. The t_{steer} is the turning time of the vehicle. W_{safe} is the reserved lateral safety distance, and its value is taken to be 2. The a_{hy} is the lateral acceleration of vehicle during driving, which, considering safety factors, does not exceed 0.85 μg; in this section, it is taken to be $a_{hy\max} = 0.6$ g. The y_f is the lateral distance of pedestrian after driving time D_{dis}/v_{hx}.

From Formula (1), the vehicle's turning time t_{steer} can be calculated, and ultimately the turning safety distance S_{steer} is obtained according to the motion state information of both the vehicle and the pedestrian:

$$S_{steer} = \left(v_{hx} - v_p \sin\theta\right) t_{steer} - \frac{1}{2} a_p t_{steer}^2 \sin\theta \quad (2)$$

When the vehicle performs a braking operation in the above road scenario, its gradually decelerates to stop with acceleration of a_{hx}. At this moment, the pedestrian is moving in an undetermined direction and at a varying speed. The following formula must be satisfied to ensure that no collision occurs between the two as they approach each other, disregarding any turning maneuvers:

$$S \geq D_{break} - [(D_{dis} - D_{break}) + D_p] + D_{safe} \tag{3}$$

Wherein the shortest braking distance D_{break} of vehicle can be expressed as

$$D_{break} = v_{hx}(\frac{0 - v_{hx}}{a_{hx}}) + \frac{1}{2}a_{hx}(\frac{0 - v_{hx}}{a_{hx}})^2 = -\frac{v_{hx}^2}{2a_{hx}} \tag{4}$$

The longitudinal displacement D_p of the pedestrian after the vehicle's braking time can be formulated as

$$D_p = v_p \sin\theta(\frac{0 - v_{hx}}{a_{hx}}) + \frac{1}{2}a_p \sin\theta(\frac{0 - v_{hx}}{a_{hx}})^2 = -\frac{v_p v_{hx} \sin\theta}{a_{hx}} + \frac{a_p v_{hx}^2 \sin\theta}{2a_{hx}^2} \tag{5}$$

In the formula, S is the longitudinal safe distance between the vehicle and the pedestrian which is necessary to avoid collision. D_{safe} is the additional longitudinal safety distance, and its value is taken to be 2. The a_{hx} is the longitudinal acceleration of the vehicle during its motion, and considering safety factors, its maximum value is taken to be $a_{hx\max} = -0.7$ g.

To provide the driver with a more operational margin during the braking process, the value of S may be small. In summary, according to Formulas (3)–(5), the braking safety distance S_{break} can be derived as

$$S_{break} = -\frac{v_{hx}^2}{a_{hx\max}} + \frac{v_p v_{hx} \sin\theta}{a_{hx\max}} - \frac{a_p v_{hx}^2 \sin\theta}{2a_{hx\max}^2} - D_{dis} + D_{safe} \tag{6}$$

2.2. Mode Determination of Collision-Avoidance Priority

As analyzed in Section 2.1, the safe distance between vehicle and pedestrian is related to the vehicle's speed, acceleration, and road-adhesion coefficient. When considering collision-avoidance operations during the interaction, it is first necessary to calculate the steering safety distance and the braking safety distance under different emergency conditions separately. To ensure as much error tolerance and as high a level of safety as possible, a higher collision-avoidance priority is assigned to the smaller of the two values.

In summary, according to the relative motion states between the host vehicle and the pedestrian, the collision-avoidance modes can be further subdivided as follows:

(1) When $D_{dis} > S_{break} > S_{steer}$ or $S_{break} > D_{dis} > S_{steer}$, the vehicle adopts a steering operation mode. In this case, if $y_f \geq 0$, the value of the steering avoidance trajectory is negative. Additionally, if $y_f < 0$, the value of the steering avoidance trajectory is positive.

(2) When $D_{dis} > S_{steer} > S_{break}$ or $S_{steer} > D_{dis} > S_{break}$, the vehicle adopts a braking operation mode. In this scenario, the vehicle continues to move along its original trajectory, and the value of the braking avoidance trajectory is 0.

The specific decision-making process for the vehicle collision-avoidance modes is shown in Figure 2.

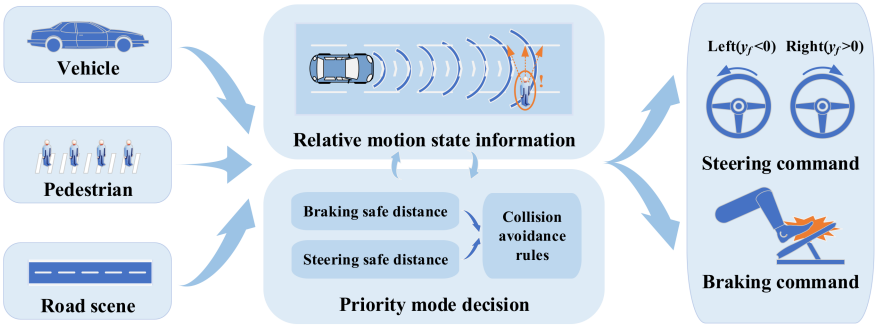

Figure 2. Flowchart of the collision-avoidance mode decision.

3. Path Planning Based on Multi-Objective Optimization

During the driving of the vehicle, after the decision-making module issues an instruction, the planning module must swiftly generate a reasonable collision-avoidance path to prevent a potential accident. Traditional path-planning methods include the Bezier curve method, A* algorithm, cell decomposition method, and view-based search method. However, these algorithms do not fully consider the dynamic characteristics of the vehicle and have inadequate constraint conditions [38].

In this section, a value function for evaluating collision-avoidance trajectories is designed, taking into account four indicators: comfort, collision-avoidance efficiency, impact of collision avoidance on traffic, and the level of collision risk. Compared to existing methods, it is able to provide more practical collision-avoidance solutions in complex traffic environments. Under the premise of ensuring safe and controllable vehicle driving conditions, the quintic polynomial method is utilized to plan collision-avoidance trajectories in vehicle–pedestrian interactions, in order to obtain optimal reference paths for steering and braking to avoid collisions.

3.1. Path Selection with Multi-Objective Optimization

To achieve a collision-avoidance path selection that considers multi-objective factors, a value function for selecting the optimal collision-avoidance trajectory is designed in this section. This function primarily takes into account the following four evaluation indicators: (1) the impact of collision avoidance on occupant comfort; (2) the efficiency of the vehicle's collision avoidance; (3) the impact of collision avoidance on traffic flow; and (4) the risk level during the collision-avoidance process.

During the collision-avoidance process, acceleration reflects the force experienced by passengers during acceleration or deceleration. The derivative of acceleration yields the jerk, which characterizes the rate of change of force. Typically, passengers may experience discomfort during acceleration or deceleration, primarily due to significant jerk. Therefore, this section defines the comfort value function J_{co} during the collision-avoidance process as follows:

$$J_{co} = \int_{t_0}^{t_1} \sqrt{Jerk_x^2(t) + Jerk_y^2(t)} \tag{7}$$

In the formula, $Jerk_x(t)$, $Jerk_y(t)$ are the longitudinal and lateral jerk of the host vehicle with respect to time t, respectively. The t_0 and t_1 are the start and end times of the collision-avoidance maneuver. A smaller value of J_{co} indicates better comfort during the collision-avoidance process.

During the driving of the vehicle, enhancing collision-avoidance efficiency not only accelerates the execution of this behavior but also improves overall safety. Furthermore, reducing the interference of the vehicle with the surrounding environment to enhance the travel efficiency of other vehicles is an important goal in the collision-avoidance process.

Therefore, the collision-avoidance efficiency value function J_{en} and the traffic impact value function J_{ef} are defined as follows:

$$\begin{cases} J_{en} = t_1 - t_0 \\ J_{ef} = x_1 - x_0 \end{cases} \tag{8}$$

In the formula, x_0 and x_1 are the longitudinal displacements at the starting and ending points of the collision-avoidance maneuver, respectively.

The construction of a safety potential field ensures that a relatively safe distance is maintained between the vehicle and the pedestrian to prevent potential accidents. Traditional Artificial Potential Fields are centered on obstacles and form circular repulsive-force zones with influence radii. However, in an interactive environment, the longitudinal speeds of vehicles are significantly greater than their lateral speeds, leading to an uneven distribution of risk levels in longitudinal and lateral areas. To better reflect the risk in an actual collision-avoidance scenario, this section modifies the repulsive potential field of a pedestrian to an elliptical shape and establishes a risk-value function that considers the safety potential field:

$$J_{po} = A_{po} \exp[-\frac{1}{2}((\frac{x - x_f}{\sigma_x})^{c_1} + (\frac{y - y_f}{\sigma_y})^{c_2})] \tag{9}$$

In the formula, A_{po} is the safety potential field coefficient for the pedestrian. The x and y are the lateral and longitudinal coordinates of any point during the vehicle's driving, respectively. The x_f and y_f are the longitudinal and lateral distances for the pedestrian after steering-time t_{steer} interval. The c_1, c_2, σ_x, and σ_y are the shape coefficients of the safety potential field.

The risk distribution, considering the safety potential field obtained from Formula (9), is shown in Figure 3.

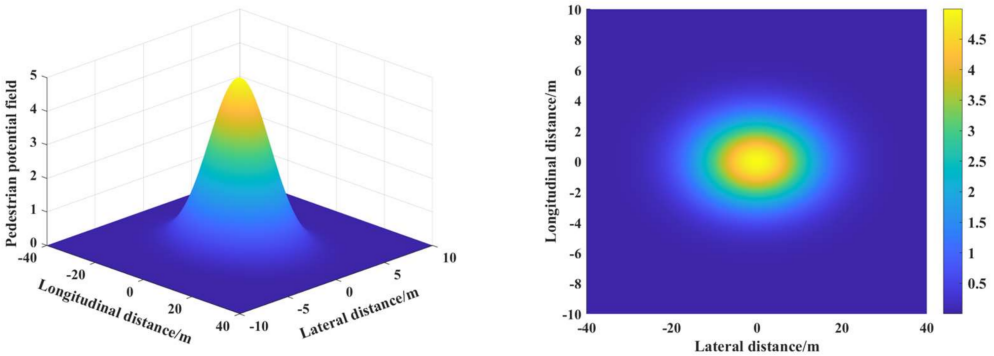

Figure 3. Risk distribution, considering the safety potential field. (**a**) 3D map of risk distribution in safety potential field. (**b**) Top map of risk distribution in safety potential field.

Taking into account the impacts of various indicators during the collision-avoidance process, a multi-objective optimization value function can be established to select the optimal trajectory from the set of collision-avoidance trajectories. In a multi-criteria evaluation system, each criterion has different weight coefficients and dimensions due to their varying nature. This study focuses on the collision-avoidance problem in the dynamic interaction between vehicle and pedestrian, in which safety is the primary concern, followed by collision-avoidance efficiency and traffic flow impact. While comfort is important, its weight is relatively small when safety, efficiency, and traffic flow are considered. Additionally, in order to solve the overall collision-avoidance value function, normalization of

the four criteria mentioned above is necessary. In this paper, the min–max normalization method is employed to process the original indicators, and based on this, a value function for multi-objective collision avoidance is designed:

$$J = \varepsilon_1\left(\frac{J_{co} - J_{co\min}}{J_{co\max} - J_{co\min}}\right) + \varepsilon_2\left(\frac{J_{en} - J_{en\min}}{J_{en\max} - J_{en\min}}\right) + \varepsilon_3\left(\frac{J_{ef} - J_{ef\min}}{J_{ef\max} - J_{ef\min}}\right) + \varepsilon_4\left(\frac{J_{po} - J_{po\min}}{J_{po\max} - J_{po\min}}\right) \tag{10}$$

In the formula, $J_{co\min}$ and $J_{co\max}$ are the minimum and maximum thresholds of the comfort value function, respectively. $J_{en\min}$ and $J_{en\max}$ are the minimum and maximum thresholds of the collision-avoidance efficiency value function, respectively. $J_{ef\min}$ and $J_{en\max}$ are the minimum and maximum thresholds of the traffic impact value function, respectively. $J_{po\min}$ and $J_{po\max}$ are the minimum and maximum thresholds of the potential field risk-value function, respectively. The ε_1, ε_2, ε_3, and ε_4 are the weight coefficients for the multi-objective collision-avoidance trajectory value function.

3.2. Path Generation of Quintic Polynomial

After designing the value function for evaluating collision-avoidance trajectories, it is necessary to establish a corresponding path-planning method to generate collision-avoidance trajectories that meet the requirements. The quintic polynomial method requires only the initial and final states of vehicle to calculate the shape of curve, and it has the advantages of being highly differentiable, continuously smooth, and highly reliable. Therefore, it is more suitable for collision-avoidance path planning in the current interactive scenario.

The expression for a quintic polynomial collision-avoidance trajectory can be represented as follows:

$$\begin{cases} x(t) = a_5t^5 + a_4t^4 + a_3t^3 + a_2t^2 + a_1t + a_0 \\ y(t) = b_5t^5 + b_4t^4 + b_3t^3 + b_2t^2 + b_1t + b_0 \end{cases} \tag{11}$$

In the formula, $x(t)$ and $y(t)$ are the longitudinal and lateral trajectory functions during the collision-avoidance process, respectively. $A = [a_5\ a_4\ a_3\ a_2\ a_1\ a_0]^T$ and $B = [b_5\ b_4\ b_3\ b_2\ b_1\ b_0]^T$ are undetermined coefficients.

By taking the first and second derivatives of vehicle's lateral and longitudinal trajectory functions, $x(t)$ and $y(t)$, the expressions for lateral and longitudinal velocities and the accelerations of the collision-avoidance vehicle can be obtained:

$$\begin{cases} \dot{x}(t) = 5a_5t^4 + 4a_4t^3 + 3a_3t^2 + 2a_2t + a_1 \\ \dot{y}(t) = 5b_5t^4 + 4b_4t^3 + 3b_3t^2 + 2b_2t + b_1 \\ \ddot{x}(t) = 20a_5t^3 + 12a_4t^2 + 6a_3t + 2a_2 \\ \ddot{y}(t) = 20b_5t^3 + 12b_4t^2 + 6b_3t + 2b_2 \end{cases} \tag{12}$$

In the formula, $\dot{x}(t)$ and $\dot{y}(t)$ are the longitudinal and lateral velocity functions during the collision-avoidance process, respectively. The $\ddot{x}(t)$ and $\ddot{y}(t)$ are the longitudinal and lateral acceleration functions during collision-avoidance process.

By further organizing Formulas (11) and (12), they can be uniformly expressed in matrix form as

$$\begin{cases} A = T\backslash X \\ B = T\backslash Y \end{cases} \tag{13}$$

In the formula, $A = [a_5\ a_4\ a_3\ a_2\ a_1\ a_0]^T$ is the longitudinal coefficient matrix. $B = [b_5\ b_4\ b_3\ b_2\ b_1\ b_0]^T$ is the lateral coefficient matrix. $X = [x_0\ \dot{x}_0\ \ddot{x}_0\ x_1\ \dot{x}_1\ \ddot{x}_1]^T$ is the longitudinal state matrix during the collision-avoidance process. $Y = [y_0\ \dot{y}_0\ \ddot{y}_0\ y_1\ \dot{y}_1\ \ddot{y}_1]^T$ is the lateral state matrix during the collision-avoidance process.

$$T = \begin{bmatrix} t_0^5 & t_0^4 & t_0^3 & t_0^2 & t_0 & 1 \\ 5t_0^4 & 4t_0^3 & 3t_0^2 & 2t_0 & 1 & 0 \\ 20t_0^3 & 12t_0^2 & 6t_0 & 2 & 0 & 0 \\ t_1^5 & t_1^4 & t_1^3 & t_1^2 & t_1 & 1 \\ 5t_1^4 & 4t_1^3 & 3t_1^2 & 2t_1 & 1 & 0 \\ 20t_1^3 & 12t_1^2 & 6t_1 & 2 & 0 & 0 \end{bmatrix}$$ is the time variable matrix during the collision-avoidance process.

In the longitudinal trajectory function $x(t)$ and the lateral trajectory function $y(t)$ of the collision-avoidance vehicle, a total of 12 unknown parameters are involved, necessitating 12 boundary conditions for their solution. By utilizing the initial state X, the final state Y, and the collision-avoidance time t of the lane-changing vehicle, the quintic polynomial of vehicle's collision-avoidance trajectory can be determined.

In the steering mode, the initial longitudinal and lateral positions of the vehicle are set to 0. According to Formula (1), to ensure that the vehicle does not collide with the pedestrian after avoidance behavior, the final longitudinal and lateral positions are determined as D_{dis} and $y_f \pm W_{safe}$, respectively. Considering that the vehicle needs to maintain its original state of motion before and after collision avoidance, the lateral velocity, longitudinal acceleration, and lateral acceleration at both the initial and final moments are set to 0. Additionally, due to the short duration of the lane change and the relatively slow speed of the pedestrian, changes in the vehicle's longitudinal velocity and the pedestrian's longitudinal position during the lane change can be neglected. Therefore, the constraints during the steering collision-avoidance process are as follows:

$$\begin{cases} x(t_0) = 0,\ \dot{x}(t_0) = v_{hx},\ \ddot{x}(t_0) = 0 \\ x(t_1) = D_{dis},\ \dot{x}(t_1) = v_{hx},\ \ddot{x}(t_1) = 0 \\ y(t_0) = 0,\ \dot{y}(t_0) = 0,\ \ddot{y}(t_0) = 0 \\ y(t_1) = y_f \pm W_{safe},\ \dot{y}(t_1) = 0,\ \ddot{y}(t_1) = 0 \end{cases} \tag{14}$$

The starting- and ending-state parameters of the primary vehicle in collision-avoidance are relatively easy to determine, but the lateral displacement y and the duration t of the collision-avoidance process are more difficult to ascertain. Therefore, a fixed-step-size traversal method within a certain range is employed to solve for these two parameters. To verify the feasibility of the decision-making and planning in steering collision-avoidance mode, the values of D_{dis}, y_f, and W_{safe} are set to 40, 0, and 1, respectively. The resulting vehicle reference path is shown in Figure 4 (The curve cluster is the feasible steering path based on quintic polynomial, and the red dashed line is the optimal steering path based on multi-objective optimization).

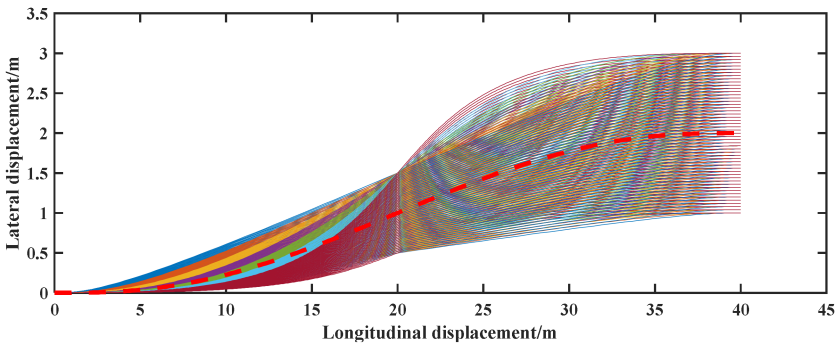

Figure 4. Reference path for collision avoidance in steering mode.

In the braking mode, the initial longitudinal and lateral positions of the vehicle are set to 0. Additionally, due to the low movement speed of the pedestrian, changes in their

longitudinal position can be ignored. According to Formula (2), to ensure that the vehicle does not collide with pedestrian after avoidance behavior, the final longitudinal position and velocity are determined as $D_{dis} - D_{safe}$ and 0, respectively. Considering that the vehicle needs to maintain its original state of motion before and after collision avoidance, the lateral velocity, longitudinal acceleration, and lateral acceleration at both the initial and final moments are all set to 0. Furthermore, since steering is not considered during the collision-avoidance process, the final lateral position is set to 0. Therefore, the constraints during braking collision-avoidance process are as follows:

$$\begin{cases} x(t_0) = 0,\ \dot{x}(t_0) = v_{hx},\ \ddot{x}(t_0) = 0 \\ x(t_1) = D_{dis} - D_{safe},\ \dot{x}(t_1) = 0,\ \ddot{x}(t_1) = 0 \\ y(t_0) = 0,\ \dot{y}(t_0) = 0,\ \ddot{y}(t_0) = 0 \\ y(t_1) = 0,\ \dot{y}(t_1) = 0,\ \ddot{y}(t_1) = 0 \end{cases} \tag{15}$$

The starting- and ending-state parameters of the main vehicle in the collision avoidance are relatively easy to determine, but the longitudinal displacement x of the vehicle and the duration t of the collision-avoidance process are difficult to determine. Therefore, for these two parameters, a fixed-step traversal method is used within a certain range to solve them. To verify the feasibility of decision planning in braking collision-avoidance mode, the values of D_{dis}, y_f, and D_{safe} are set to 40, 0, and 2, respectively. The calculated vehicle reference path is shown in Figure 5 (The curve cluster is the feasible braking path based on the quintic polynomial, and the red dashed line is the optimal braking path based on multi-objective optimization).

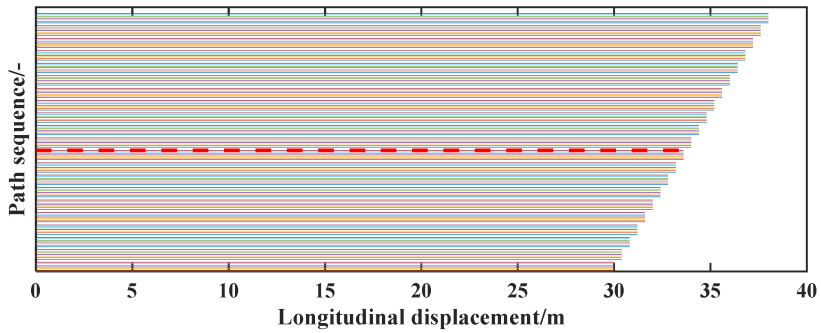

Figure 5. Reference path for collision avoidance in braking mode.

4. Collision-Avoidance Control Based on Stratified Strategy

During the driving of the vehicle, to ensure timely and effective collision avoidance, the control module must respond rapidly and track the optimal collision-avoidance trajectory in real-time. SMC, known for its rapid response, high robustness, and excellent anti-interference and fault-tolerant capabilities, can quickly stabilize the states of complex dynamic systems within a limited time [39]. However, when the system state approaches a sliding surface, the high-frequency switching and discontinuous nature of the control input can lead to oscillations. The RBF algorithm can address the aforementioned issues through updating and learning processes. It possesses strong local nonlinear approximation capabilities, enabling effective handling of system uncertainties and external disturbances. Therefore, this section optimizes the traditional SMC using the RBF algorithm to further enhance the control accuracy, adaptability, and system stability for lateral collision avoidance. Furthermore, an FD-SF algorithm is designed according to actual requirements to achieve precise tracking of the longitudinal collision-avoidance path.

To implement steering-based collision-avoidance control for a vehicle, it is first necessary to establish an equivalent dynamic model. Since the effect of steering on the vertical

motion is minimal, the influence of the suspension system is neglected. By considering the vehicle's lateral motion and yaw motion, the full vehicle model is simplified into a linear two-degree-of-freedom model, as shown in Figure 6.

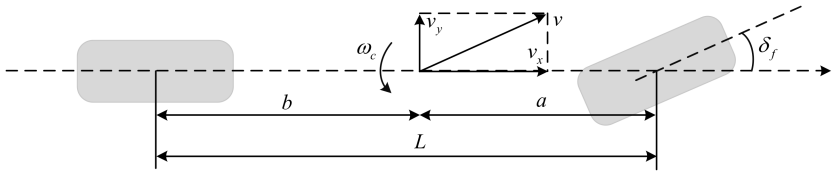

Figure 6. Equivalent vehicle dynamic model.

In Figure 6, v_x and v_y are the longitudinal and lateral velocities of the vehicle during its motion, respectively. The $\dot{\omega}_c$ is the yaw rate of the vehicle during its motion. The δ_f is the steering angle of front wheels. The a and b are the distances from vehicle's center of mass to the front and rear axles, respectively. L is the wheelbase of the vehicle.

Therefore, the differential equation for the vehicle's equivalent dynamic model is given by

$$\begin{cases} \dot{v}_y = \frac{-2(C_f+C_r)}{mv_x}v_y + \frac{-2(C_f a - C_r b)}{mv_x}\omega_c + v_x\omega_c + \frac{2C_f}{m}\delta_f \\ \dot{\omega}_c = \frac{-2(aC_f - bC_r)}{Iv_x}v_y + \frac{-2(a^2C_f + b^2C_r)}{Iv_x}\omega_c + \frac{2aC_f}{I}\delta_f \end{cases} \tag{16}$$

In the formula, m is the vehicle's total mass. C_f and C_r are the lateral stiffnesses of the front and rear tires, respectively.

By further simplifying Formula (16), the following equation is obtained:

$$\begin{cases} \dot{v}_y = f_1 + g_1\delta_f \\ \dot{\omega}_c = f_2 + g_2\delta_f \end{cases} \tag{17}$$

Wherein,
$f_1 = \frac{-2(C_f+C_r)}{mv_x}v_y + \frac{-2(aC_f-bC_r)}{mv_x}\omega_c + v_x\omega_c$, $f_2 = \frac{-2(aC_f-bC_r)}{Iv_x}v_y + \frac{-2(a^2C_f+b^2C_r)}{Iv_x}\omega_c$, $g_1 = \frac{2C_f}{m}u$, $g_2 = \frac{2aC_f}{I}u$,$u = \delta_f$.

The design of the sliding mode controller aims to ensure stable tracking of the desired yaw rate by adjusting the yaw rate of vehicle's center of mass, thereby achieving real-time tracking of the desired trajectory. The desired yaw rate change rate $\dot{\omega}_r$ and the desired yaw rate ω_r for the vehicle are

$$\begin{cases} \dot{\omega}_r = \dot{v}_c\gamma + v_c\dot{\gamma} \\ \omega_r = \omega_c + \kappa\dot{\omega}_r \end{cases} \tag{18}$$

Wherein, the curvature change rate $\dot{\gamma}$ of the reference path at the vehicle's current point is

$$\dot{\gamma} = \frac{d\left[\frac{\ddot{y}}{(1+\dot{y})^{3/2}}\right]}{dx}\frac{dx}{dt} = v_c\frac{\dddot{y}(1+\dot{y}^2) - 3\ddot{y}^2\dot{y}}{(1+\dot{y}^2)^{5/2}} \tag{19}$$

In the formula, v_c is the vehicle's center-of-mass velocity. κ is the scaling factor.

Therefore, the design of the switching function is as follows:

$$\begin{cases} s(t) = ce(t) = c(\omega_r - \omega_c) \\ \dot{s}(t) = c\dot{e}(t) = c(\dot{\omega}_r - f_2 - g\delta_f) \end{cases} \tag{20}$$

In the formula, $e(t)$ is the system control error. ω_r is the reference yaw rate.

Traditional sliding mode motion consists of two processes: approaching motion and sliding mode motion. To ensure that the system state approaches the sliding surface rapidly,

the exponential approaching law $\dot{s} = -k\text{sgn}(s)$, $k > 0$ is selected, and then the ideal control input of the sliding mode controller is obtained as follows:

$$u_{st} = \delta_f = \left(c\dot{e} + \ddot{\omega}_r - f_2 + k\text{sgn}(s)\right)/g \tag{21}$$

To improve path-tracking accuracy and address the issue of degraded control performance due to chattering in traditional sliding mode control, this paper introduces the RBF neural network algorithm to optimize sliding mode control. The control law of the RBF-SMC algorithm consists of equivalent control u_{eq} and switching control u_{sw}. Firstly, to keep the system state on the sliding surface, the condition $\dot{s} = 0$ must be satisfied, from which the equivalent control input u_{eq} can be derived as

$$u_{eq} = \delta_{eq} = \left(c\dot{e} + \ddot{\omega}_r - f_2\right)/g \tag{22}$$

The chattering problem in sliding mode control is mainly caused by the switching control law, and the design quality of the switching control law directly affects control accuracy and chattering intensity. Therefore, this section employs the RBF algorithm to design a switching control law.

The RBF neural network consists of three layers: input layer, hidden layer, and output layer. Wherein, the input layer is $X^* = [x_1, x_2, \cdots, x_n]^T$, the radial basis vectors of hidden layer are $H = [h_1, h_2, \cdots, h_n]^T$, and the connection from input layer to hidden layer is through a Gaussian basis function, that is,

$$h_j = \exp(-\frac{\left\|X - c_j\right\|^2}{2b_j^2}), j = 1, \cdots, m \tag{23}$$

In the formula, $C = [c_{j1}, c_{j2}, c_{j3} \cdots c_{jn}]$ represents the center vectors of nodes in the neural network. $B = [b_1, b_2, b_3 \cdots b_j]$ represents the width vectors of basis functions of nodes in the neural network.

Let the weight vector from hidden layer to output layer be denoted as $W = [w_1, w_2, w_3 \cdots w_j]$; then, the output of RBF neural network is given by

$$y(t) = w_1 h_1 + w_2 h_2 + w_3 h_3 + \cdots w_j h_j \tag{24}$$

The relevant parameters of the neural network are continuously adjusted through the gradient descent method to minimize error between the network's output value and actual value.

To ensure that the system state slides along sliding mode surface, it is necessary to guarantee that $s(t)\dot{s}(t) < 0$. Based on the above analysis, this section takes the switching function and its derivative as inputs to the RBF neural network, and uses the output of neural network as the switching control input u_{sw}, that is,

$$u_{sw} = \delta_{sw} = W^T H = \sum_{j=1}^{m} w_j \exp(-\frac{\left\|s - c_j\right\|^2}{2b_j^2}) \tag{25}$$

The learning index of the RBF neural network is set to $E = s(t)\dot{s}(t)$, and real-time training of network parameters is conducted using the gradient descent method, resulting in the following:

$$\begin{cases} w_j(t+1) = w_j(t) + dw_j + \alpha(w_j(t) + w_j(t-1)) \\ dw_j = -\frac{\partial E}{\partial w_j} = -\frac{\partial \dot{s}(t)s(t)}{\partial u(t)}\frac{\partial u(t)}{\partial w_j} = -\eta g s(t)\exp(-\frac{\left\|x - c_j\right\|^2}{2b_j^2}) = \gamma s(t) h_j \end{cases} \tag{26}$$

$$\begin{cases} c_{ij}(t+1) = c_{ij}(t) + dc_{ij} + \alpha(c_j(t) + c_{ij}(t-1)) \\ dc_{ij} = -\frac{\partial E}{\partial c_{ij}} = -\eta g s(t) w_j h_j \frac{\|x_j - c_{ij}\|^2}{b_j^3} = \gamma s(t) w_j h_j \frac{\|x_j - c_{ij}\|^2}{b_j^3} \end{cases} \quad (27)$$

$$\begin{cases} b_j(t+1) = b_j(t) + db_j + \alpha(b_j(t) + b_j(t-1)) \\ db_j = -\frac{\partial E}{\partial b_j} = -\eta g s(t) w_j h_j \frac{\|x - c_j\|^2}{b_j^3} = \gamma s(t) w_j h_j \frac{\|x - c_j\|^2}{b_j^3} \end{cases} \quad (28)$$

In the formula, dw_j, dc_{ij}, and db_j are the rates of change for network weights, centers, and basis widths, respectively. The α is the learning factor, η is the momentum factor, and γ is the integration parameter.

In summary, the total control input based on the RBF-SMC algorithm can be expressed as

$$u_{st} = u_{eq} + u_{sw} = \delta_{eq} + \delta_{sw} \quad (29)$$

The pseudocode for the lateral tracking control is shown in Algorithm 1.

Algorithm 1 Lateral tracking control of RBF-SMC

Input: Yaw rate; Vehicle speed
Output: Front wheel steering angle
Step 1. Initialize control parameters
1. Initialize the weights, centers, and scaling factors of the RBF network
2. Set control parameters and initial conditions
Step 2. Calculate RBF-SMC control
1. Apply sliding mode surface function based on error (16)–(22)
2. Optimize control signals using radial basis function (23)–(25)
Step 3. Update parameters and return control outputs
1. Adjusting parameters in RBF network based on learning rate (26)–(28)
2. Output the control signal calculated by the RBF-SMC controller (29)

For the braking-based collision-avoidance control of the vehicle, the ideal longitudinal velocity v_{hx}^* can be directly determined through path planning. Based on this, combined with the vehicle's driving force demand and velocity feedback theory [40], the ideal wheel braking control force F_{br} can be further derived:

$$F_{br} = -mg\sin\varphi - mgf\cos\varphi - \frac{AC_D v_{hx}^2}{21.15} + \tau m a_{hx} + H(v_{hx}^* - v_{hx}) \quad (30)$$

In the formula, g is the gravitational acceleration. The φ is the road gradient. The f is the rolling resistance coefficient. A is the frontal area. C_D is the air resistance coefficient. The τ is the vehicle's rotational mass conversion factor. H is the longitudinal velocity feedback coefficient, which can be determined by the Proportional–Integral–Derivative control algorithm.

The main parameters of the collision-avoidance control are shown in Table 2.

Based on the above analysis, a collision-avoidance control for the vehicle can be implemented. The controller takes the ideal yaw rate and braking acceleration as inputs and calculates the required yaw angle and braking torque for tracking target trajectory through corresponding algorithms. The control process is shown in Figure 7.

Table 2. Parameters of the collision-avoidance control.

Controller Parameters	Values
Vehicle mass (m)	1270 kg
Distance from front axle to centroid (a)	1.05 m
Distance from rear axle to centroid (b)	1.61 m
Yaw moment of inertia	2060 kg·m^2
Sliding mode parameters (c)	15
Control rate (k)	40
Learning factor (α)	0.01
Momentum factor (η)	0.2

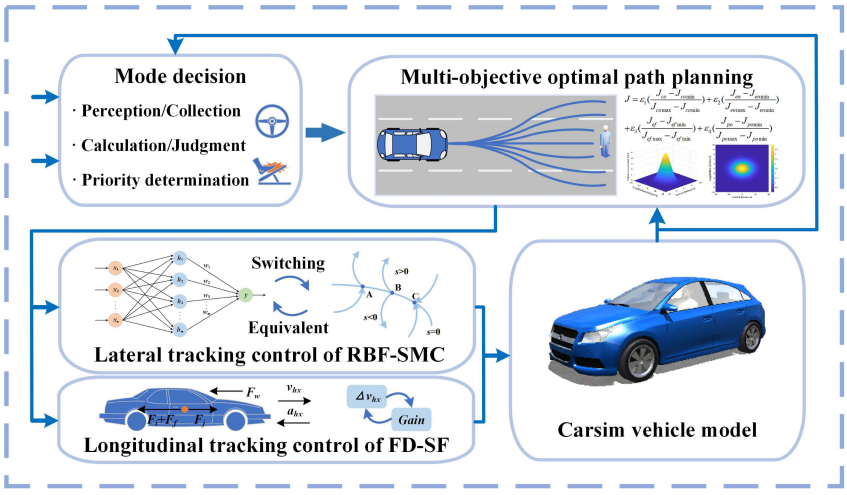

Figure 7. Flowchart of decision planning and tracking control.

5. Verification of Collision-Avoidance Control Strategy Effects

To verify the effectiveness of the proposed strategy, the vehicle–pedestrian interaction scenario is constructed through co-simulation using Carsim and Simulink in this study. Various driving conditions are set to test and analyze the collision-avoidance control effects based on decision and planning.

5.1. Vehicle–Pedestrian Interaction Scenario 1

The ground adhesion coefficient is set to 0.85, with the host vehicle initially driving at speed of 40 km/h along a straight road. At distance of 40 m ahead, a pedestrian rapidly crosses the road from a point −4 m away from the centerline, moving at a speed of 2 m/s, and with an acceleration of 0.2 m/s^2, forming a −30° angle with the *y*-axis. The simulation results for this scenario are shown in Figure 8.

As shown in Figure 8, when a pedestrian suddenly appears ahead during the driving of the vehicle, the decision-making module generates a braking command according to the actual situation and priority rule. Upon receiving corresponding command, the planning module swiftly generates a cluster of collision-avoidance paths (curve clusters) that meet the current demand and selects the optimal braking reference path (red line) through a multi-objective optimized value function, as shown in Figure 8a. Under a collision-avoidance control based on the FD-SF approach, the vehicle drives steadily along the desired path. Both the longitudinal velocity and displacement remain within the ideal range, with maximum deviations of 0.21 m/s and 0.11 m, respectively. These results demonstrate that the collision-avoidance control strategy based on decision and planning can effectively identify and generate an optimal braking path that meets the obstacle-avoidance conditions. At the same time, it ensures that vehicle drives steadily along the

expected path, thereby significantly reducing the potential risk of collision between the vehicle and the pedestrian.

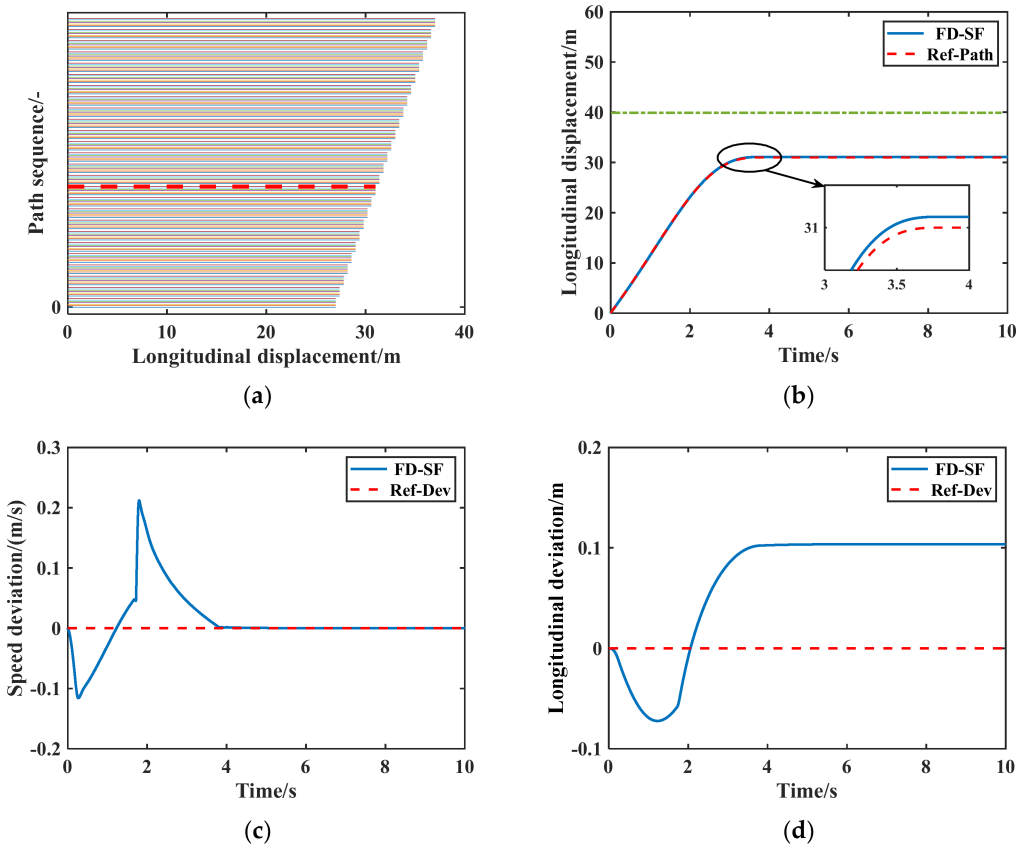

Figure 8. Collision-avoidance control results for scenario 1. (**a**) Planned path, (**b**) Driving path, (**c**) Speed deviation, (**d**) Longitudinal deviation.

5.2. Vehicle–Pedestrian Interaction Scenario 2

The ground adhesion coefficient is set to 0.85, with the host vehicle initially driving at speed of 60 km/h along a straight road. At distance of 30 m ahead, a pedestrian rapidly crosses road from a point −4 m away from the centerline, moving at a speed of 3 m/s and an acceleration of 0.3 m/s^2, forming a 30° angle with the *y*-axis. The simulation results for this scenario are shown in Figure 9.

As shown in Figure 9, when a pedestrian suddenly appears in front of vehicle during its drive, the decision-making module generates a steering command according to the actual situation and priority rule. Upon receiving the corresponding command, the planning module swiftly generates a cluster of collision-avoidance paths (curve clusters) that meet the current demand and selects the optimal steering reference path (red dashed line) through a multi-objective optimized value function, as shown in Figure 9a. Under the control of collision avoidance using both EFF-SMC and RBF-SMC, the vehicle drives steadily along the expected path. The yaw rate and lateral displacement both remain within their ideal ranges. Compared to the maximum yaw rate deviation of 0.003 rad/s and the maximum lateral displacement deviation of −0.113 m under EFF-SMC control, the deviations under RBF-SMC control are reduced to 0.001 rad/s and −0.051 m, respectively, with tracking efficiency improvements of 66.7% and 54.9%. These results demonstrate that the collision-avoidance control strategy based on decision and planning can generate an optimal steering path that meets obstacle-avoidance conditions, ensuring that the vehicle drives along the expected path in a stable manner. Furthermore, RBF-SMC control exhibits superior performance in terms of tracking accuracy.

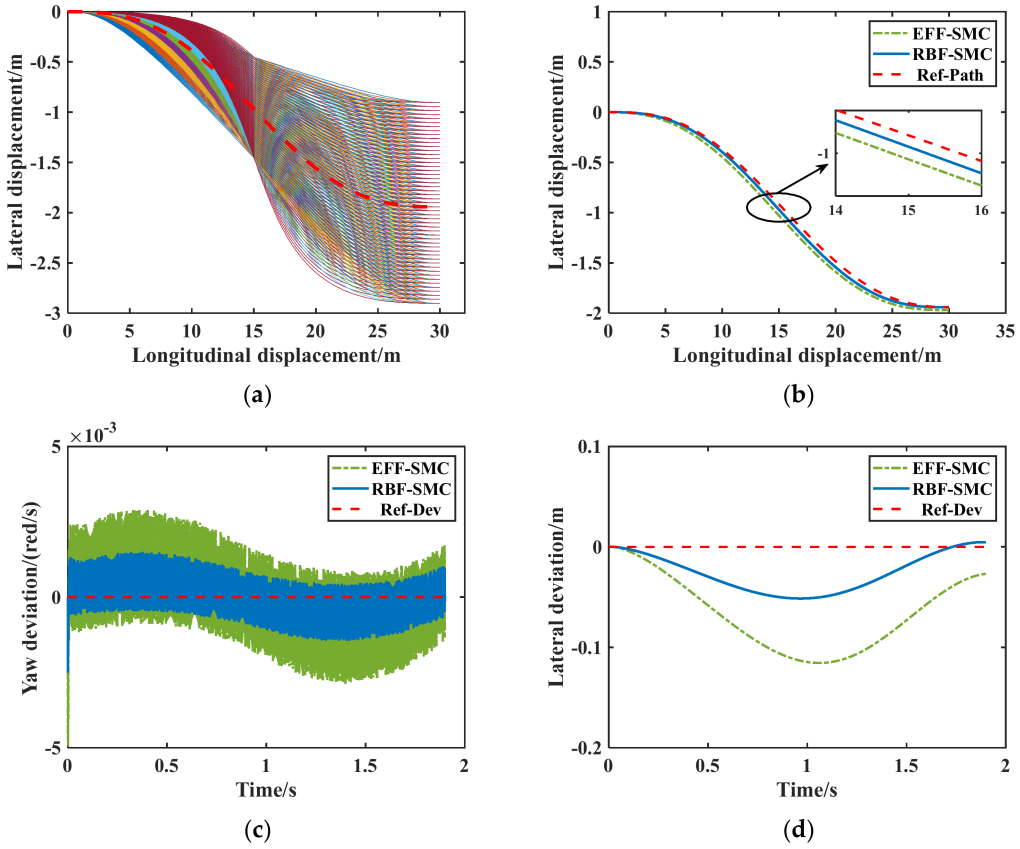

Figure 9. Collision-avoidance control results for scenario 2. (**a**) Planned path; (**b**) Driving path; (**c**) Yaw deviation; (**d**) Lateral deviation.

5.3. Vehicle–Pedestrian Interaction Scenario 3

The ground adhesion coefficient is set to 0.85, with the host vehicle initially driving at speed of 80 km/h along a straight road. At distance of 25 m ahead, a pedestrian rapidly crosses road from a point −4 m away from the centerline, moving at a speed of 4 m/s and an acceleration of 0.4 m/s^2, forming a 30° angle with the y-axis. The simulation results for this scenario are shown in Figure 10.

As shown in Figure 10, a pedestrian suddenly appears in front of vehicle during its drive. The decision-making module generates a steering command according to the actual situation and priority rule. Upon receiving the command, the planning module swiftly generates a cluster of collision-avoidance paths (curve clusters) that meet the current requirements and selects the optimal steering reference path (red dashed line) through a multi-objective optimized value function, as shown in Figure 10a. Under the influence of collision-avoidance control based on EFF-SMC and RBF-SMC, the vehicle is able to stably follow the expected path. Due to the initial high speed, the tracking accuracy for the yaw rate momentarily decreases and then gradually stabilizes after a slight overshoot. Relative to the maximum deviations of 0.008 rad/s in yaw rate and 0.104 m in lateral displacement under EFF-SMC control, the deviations under RBF-SMC control are reduced to 0.004 rad/s and 0.054 m, respectively, with tracking efficiency improvements of 50.0% and 48.1%. These results indicate that the strategy can generate an optimal steering path that meets the obstacle-avoidance conditions, ensuring stable path-tracking by the vehicle. Furthermore, RBF-SMC control demonstrates superior performance in terms of tracking accuracy.

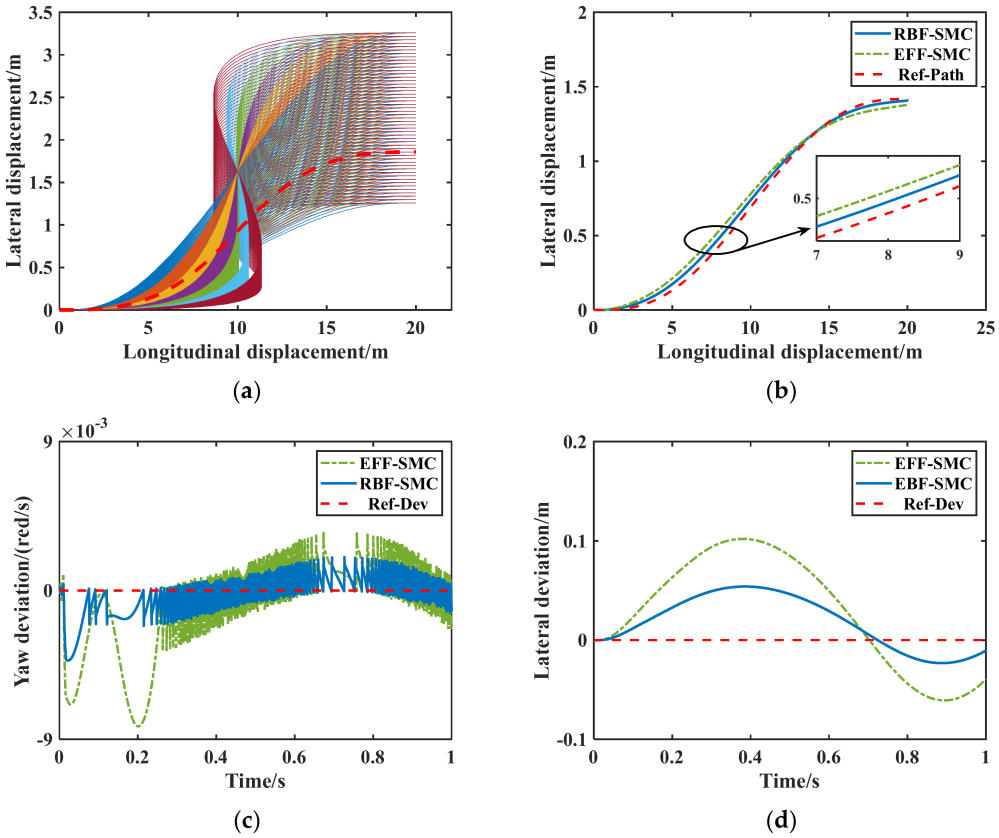

Figure 10. Collision-avoidance control results for scenario 3. (**a**) Planned path; (**b**) Driving path; (**c**) Yaw deviation; (**d**) Lateral deviation.

6. Conclusions

This study proposes an collision-avoidance control strategy based on emergency decisions and planning for a vehicle–pedestrian interaction. Firstly, by analyzing the potential collision risks faced by both entities during dynamic interactions, the corresponding safe distances are calculated, and decisions as to steering or braking are made based on a priority-mode rule. Secondly, a quintic polynomial method is employed to generate a smooth and controllable cluster of collision-avoidance trajectories, which are then evaluated and selected based on a multi-objective optimized value function. Furthermore, the traditional sliding mode control has been optimized through the RBF-SMC algorithm, enhancing the accuracy and system stability of collision-avoidance control. Additionally, an FD-SF algorithm is designed to achieve precise tracking of the longitudinal braking trajectory. The results demonstrate that the proposed strategy exhibits excellent collision-avoidance performance under various conditions. In different collision-avoidance modes, the vehicle can accurately make decisions, plan, and track the optimal collision-avoidance path. Moreover, under the control strategy optimized by RBF-SMC, tracking accuracy and system response speed are significantly improved.

In conclusion, the method proposed in this paper provides an efficient and robust solution for autonomous and assisted-driving systems. It can adjust the vehicle's trajectory in real time and with precision in dynamic vehicle–pedestrian-interaction environments, effectively preventing collision accidents and enhancing traffic mobility and safety. Consequently, it provides effective technical support for the sustainable development of complex transportation scenarios, yielding significant social and environmental benefits. However, the current decision and planning methods do not fully account for more complex pedestrian behavior. Additionally, external noise may reduce the control performance, necessitating improvements to the RBF-SMC algorithm to enhance its robustness. Finally, in real-time

applications, the algorithm may face computational delays. Future research will incorporate additional pedestrian-behavior variables, optimize the algorithm's adaptability and real-time updating capabilities, and consider additional road conditions and environmental factors to further improve the intelligence and flexibility of collision-avoidance control.

Author Contributions: Conceptualization, Z.H. and J.R.; methodology, Z.H.; software, Z.H.; validation, Z.H.; formal analysis, Z.H.; investigation, J.R.; resources, J.R.; data curation, Z.H.; writing—original draft preparation, Z.H.; writing—review and editing, J.R., Y.L., H.W., Z.X. and J.Z.; funding acquisition, J.R. All authors have read and agreed to the published version of the manuscript.

Funding: This research received no external funding.

Institutional Review Board Statement: Not applicable.

Informed Consent Statement: Not applicable.

Data Availability Statement: The datasets used and analyzed during the current study are available.

Acknowledgments: The authors would like to express their gratitude to all those who have contributed to this research.

Conflicts of Interest: All authors certify that they have no affiliations with or involvement in any organization or entity with any financial interest or non-financial interest in the subject matter or materials discussed in this manuscript.

References

1. Noh, S.; An, K. Decision-making framework for automated driving in highway environments. *IEEE Trans. Intell. Transp. Syst.* **2017**, *19*, 58–71. [CrossRef]
2. Shetty, A.; Yu, M.; Kurzhanskiy, A.; Grembek, O.; Tavafoghy, H.; Varayia, P. Safety challenges for autonomous vehicles in the absence of connectivity. *Transp. Res. Part C Emerg. Technol.* **2021**, *128*, 103133. [CrossRef]
3. Pek, C.; Manzinger, S.; Koschi, M.; Althoff, M. Using online verification to prevent autonomous vehicles from causing accidents. *Nat. Mach. Intell.* **2020**, *2*, 518–528. [CrossRef]
4. Codevilla, F.; Muller, M.; Lopez, A.; Koltun, V.; Dovovitskiy, A. End-to-end driving via conditional imitation learning. In Proceedings of the 2018 IEEE International Conference on Robotics and Automation (ICRA), Brisbane, QLD, Australia, 21–25 May 2018; pp. 4693–4700.
5. Chu, H.; Guo, L.; Yan, Y.; Gao, B.; Chen, H. Self-learning optimal cruise control based on individual car-following style. *IEEE Trans. Intell. Transp. Syst.* **2020**, *22*, 6622–6633. [CrossRef]
6. Liu, Y.; Wang, X.; Li, L.; Cheng, S.; Chen, Z. A novel lane change decision-making model of autonomous vehicle based on support vector machine. *IEEE Access* **2019**, *7*, 26543–26550. [CrossRef]
7. Dou, Y.; Yan, F.; Feng, D. Lane changing prediction at highway lane drops using support vector machine and artificial neural network classifiers. In Proceedings of the 2016 IEEE International Conference on Advanced Intelligent Mechatronics (AIM), Banff, AB, Canada, 12–15 July 2016; pp. 901–906.
8. Zhang, Y.; Gao, B.; Guo, L.; Guo, H.; Chen, H. Adaptive decision-making for automated vehicles under roundabout scenarios using optimization embedded reinforcement learning. *IEEE Trans. Neural Netw. Learn. Syst.* **2020**, *32*, 5526–5538. [CrossRef]
9. Varga, B.; Brand, T.; Schmitz, M.; Hashemi, E. Interaction-Aware Model Predictive Decision-Making for Socially-Compliant Autonomous Driving in Mixed Urban Traffic Scenarios. *SSRN* **2024**, 5014033. [CrossRef]
10. Varga, B.; Yang, D.; Martin, M.; Hohmann, S. Cooperative decision-making in shared spaces: Making urban traffic safer through human-machine cooperation. In Proceedings of the 2023 IEEE 21st Jubilee International Symposium on Intelligent Systems and Informatics (SISY), Pula, Croatia, 21–23 September 2023; pp. 109–114.
11. Wang, J.; Zhang, Q.; Zhao, D.; Chen, Y. Lane change decision-making through deep reinforcement learning with rule-based constraints. In Proceedings of the 2019 International Joint Conference on Neural Networks (IJCNN), Budapest, Hungary, 14–19 July 2019; pp. 1–6.
12. Wolf, P.; Hubschneider, C.; Weber, M.; Bauer, A.; Hartl, J.; Durr, F. Learning how to drive in a real world simulation with deep q-networks. In Proceedings of the 2017 IEEE Intelligent Vehicles Symposium (IV), Los Angeles, CA, USA, 11–14 June 2017; pp. 244–250.
13. Liao, J.; Liu, T.; Tang, X.; Mu, X.; Huang, B.; Cao, D. Decision-making strategy on highway for autonomous vehicles using deep reinforcement learning. *IEEE Access* **2020**, *8*, 177804–177814. [CrossRef]
14. Song, X.; Cao, H.; Huang, J. Vehicle path planning in various driving situations based on the elastic band theory for highway collision avoidance. *Proc. Inst. Mech. Eng. Part D J. Automob. Eng.* **2013**, *227*, 1706–1722. [CrossRef]

15. Woo, H.; Ji, Y.; Kono, H.; Tamura, Y.; Kuroda, Y.; Sugano, T.; Yamamoto, Y.; Asama, H. Automatic detection method of lane-changing intentions based on relationship with adjacent vehicles using artificial potential fields. *Int. J. Automot. Eng.* **2016**, *7*, 127–134. [CrossRef]
16. Li, G.; Yang, Y.; Zhang, T.; Zhang, T.; Qu, X.; Cao, D.; Cheng, B. Risk assessment based collision avoidance decision-making for autonomous vehicles in multi-scenarios. *Transp. Res. Part C Emerg. Technol.* **2021**, *122*, 102820. [CrossRef]
17. Chen, H.; Wang, J. A Decision-making Method for Lane Changes of Automated Vehicles on Freeways Based on Drivers' Dissatisfaction. *China J. Highw. Transp.* **2019**, *32*, 1–9, 45.
18. Li, C.; Lu, S.; Zhang, B.; Wu, W.; Lu, J. Human-vehicle Steering Collision Avoidance Path Planning Based on Pedestrian Location Prediction. *Automot. Eng.* **2021**, *43*, 877–884.
19. Wang, J.; Li, B.; Meng, Q.H. Kinematic Constrained Bi-directional RRT with Efficient Branch Pruning for Robot Path Planning. *Expert Syst. Appl.* **2020**, *170*, 114541. [CrossRef]
20. Maseko, B.B.; Van Daalen, C.E.; Treurnicht, J. Optimised Informed RRTs for Mobile Robot Path Planning. *IFAC-PapersOnLine* **2021**, *54*, 157–162. [CrossRef]
21. Zhou, Y.; Zhang, E.; Guo, H.; Fang, Y.; Li, H. Lifting path planning of mobile cranes based on an improved RRT algorithm. *Adv. Eng. Inform.* **2021**, *50*, 101376. [CrossRef]
22. Hu, M.; Mou, B.; Yang, Z.; Bian, Y.; Qing, X. A Hybrid A* Path Planning Method Based on DBSCAN and Dichotomy. *Automot. Eng.* **2023**, *45*, 341–349, 371.
23. Hu, Y.; Tian, B.; Chen, W.; Zhang, R. Obstacle Avoidance Trajectory Planning for Intelligent Vehicle Based on Derived State Lattice from Obstacle. *Automot. Eng.* **2019**, *41*, 967–974.
24. Ji, J.; Khajepour, A.; Melek, W.W.; Huang, Y. Path planning and tracking for vehicle collision avoidance based on model predictive control with multiconstraints. *IEEE Trans. Veh. Technol.* **2016**, *66*, 952–964. [CrossRef]
25. Ren, J.; McIsaac, K.A.; Patel, R.V. Modified Newton's method applied to potential field-based navigation for mobile robots. *IEEE Trans. Robot.* **2006**, *22*, 384–391.
26. Sudhakara, P.; Ganapathy, V.; Priyadharshini, B.; Sundaran, K. Obstacle avoidance and navigation planning of a wheeled mobile robot using amended artificial potential field method. *Procedia Comput. Sci.* **2018**, *133*, 998–1004. [CrossRef]
27. Zhu, B.; Yan, S.; Zhao, J.; Deng, W. Personalized lane-change assistance system with driver behavior identification. *IEEE Trans. Veh. Technol.* **2018**, *67*, 10293–10306. [CrossRef]
28. Suh, J.; Chae, H.; Yi, K. Stochastic model-predictive control for lane change decision of automated driving vehicles. *IEEE Trans. Veh. Technol.* **2018**, *67*, 4771–4782. [CrossRef]
29. Wei, C.; Li, S. Planning a Continuous Vehicle Trajectory for an Automated Lane Change Maneuver by Nonlinear Programming considering Car-Following Rule and Curved Roads. *J. Adv. Transp.* **2020**, *2020*, 8867447. [CrossRef]
30. Xiong, L.; Yang, X.; Zhuo, G.; Leng, B.; Zhang, R. Review on Motion Control of Autonomous Vehicles. *J. Mech. Eng.* **2020**, *56*, 127–143.
31. Liu, Z.; Chen, J.; Lan, F.; Xia, H. Methodology of hierarchical collision avoidance for high-speed self-driving vehicle based on motion-decoupled extraction of scenarios. *IET Intell. Transp. Syst.* **2020**, *14*, 172–181. [CrossRef]
32. Han, Z.; Lu, Y.; Li, H.; Zhang, J. Research on intelligent optimal allocation control strategy for stability and braking of heavy tyre blowout vehicle. *Proc. Inst. Mech. Eng. Part K J. Multi-Body Dyn.* **2024**, *238*, 524–538. [CrossRef]
33. Xu, S.; Peng, H. Design, analysis, and experiments of preview path tracking control for autonomous vehicles. *IEEE Trans. Intell. Transp. Syst.* **2020**, *21*, 48–58. [CrossRef]
34. Yu, Z.; Zhang, R.; Xiong, L.; Huang, C. Dynamic Control for Unmanned Skid-steering Vehicle with Conditional Integartors. *J. Mech. Eng.* **2017**, *53*, 29–38. [CrossRef]
35. Liu, T.; Shen, Y.; Wang, K. Path tracking control for autonomous truck with dual modular chassis. *Automot. Innov.* **2023**, *6*, 558–570. [CrossRef]
36. Nam, H.; Choi, W.; Ahn, C. Model predictive control for evasive steering of an autonomous vehicle. *Int. J. Automot. Technol.* **2019**, *20*, 1033–1042. [CrossRef]
37. Lu, Y.; Han, Z.; Zhang, J.; Li, Y. Collaborative control of trajectory tracking and braking stability of intelligent vehicles with a blowout tire. *J. Mech. Sci. Technol.* **2024**, *38*, 67–78. [CrossRef]
38. Katrakazas, C.; Mohammed, Q.; Chen, W.; Deka, L. Real-time motion planning methods for autonomous on-road driving: State-of-the-art and future research directions. *Transp. Res. Part C Emerg. Technol.* **2015**, *60*, 416–442. [CrossRef]
39. Sabiha, A.D.; Kamel, M.A.; Said, E.; Hussein, W.M. ROS-based trajectory tracking control for autonomous tracked vehicle using optimized backstepping and sliding mode control. *Robot. Auton. Syst.* **2022**, *152*, 104058. [CrossRef]
40. Cui, H.; Ruan, J.; Wu, C.; Zhang, K.; Li, T. Advanced deep deterministic policy gradient based energy management strategy design for dual-motor four-wheel-drive electric vehicle. *Mech. Mach. Theory* **2023**, *179*, 105119. [CrossRef]

Disclaimer/Publisher's Note: The statements, opinions and data contained in all publications are solely those of the individual author(s) and contributor(s) and not of MDPI and/or the editor(s). MDPI and/or the editor(s) disclaim responsibility for any injury to people or property resulting from any ideas, methods, instructions or products referred to in the content.